Investigation of Alloy-Dependent Occurrence of Ferromagnetism in Carbon-Expanded Austenitic Steel after Low-Temperature Surface Hardening

Philipp Schuler,* Ulrich Krupp, Paul Gümpel, Joachim Mayer, Alexander Schwedt, and Anke Aretz

Ferromagnetism is of increasing importance in the growing field of electromobility and data storage. In stable austenitic steels, the occurrence of ferromagnetism is not expected and would also interfere with many applications. However, ferromagnetism in austenitic stainless steels after low-temperature nitriding has already been shown in the past. Herein, the presence of ferromagnetism in austenitic steels is discovered after low-temperature carburization (Kolsterizing), which represents a novel and unique finding. A zone of expanded austenite is established on various austenitic stainless steels by low-temperature carburization and the respective ferromagnetism is investigated in relation to the alloy composition. The ferromagnetism occurring is determined by means of a commercial magnetoinductive sensor (Feritscope). Ferromagnetic domains are visualized by magnetic force microscopy and a ferrofluid. X-ray diffraction measurements indicate a clear difference in the lattice expansion of the different alloys. Furthermore, a different appearance of the magnetizable microstructure regions (magnetic domain structure) is detected depending on the grain orientation determined by electron backscatter diffraction (EBSD). Strongly pronounced magnetic domains show no linear lattice defects, whereas in small magnetizable areas linear lattice defects are detected by electron channeling contrast imaging and EBSD.

P. Schuler, U. Krupp
IEHK Institute
RWTH Aachen University
Intzestraße 1, 52072 Aachen, Germany
E-mail: p.schuler@witg.ch

P. Gümpel
Institute for Materials System Technology Thurgau
Konstanzer Strasse 19, 8274 Tägerwilen, Switzerland

J. Mayer, A. Schwedt, A. Aretz
GfE Central Facility for Electron Microscopy
RWTH Aachen University
Ahornstraße 55, 52074 Aachen, Germany

The ORCID identification number(s) for the author(s) of this article can be found under https://doi.org/10.1002/srin.202100272.

1. Introduction

Due to a chromium content of at least 12 wt %, along with a low carbon content to prevent chromium binding by carbide formation, austenitic stainless steels have very good corrosion resistance.[1] The free chromium content results in a passive layer (oxide layer) of a few nanometers and protects the steel from the surrounding medium.[2] Based on the high content of austenite-stabilizing alloying elements, the face-centered cubic (fcc) lattice structure is maintained below room temperature. Due to the lack of fcc to body-centered cubic (bcc) transformation, conventional hardening processes are not applicable. In the annealed condition, the hardness of these alloys is very low due to the fcc lattice structure, and accordingly, they can only be used to a limited extent in tribological stressing. By means of low-temperature surface hardening, it is possible to harden such steels on the surface and thereby achieve improved wear resistance while maintaining excellent corrosion resistance.[3,4] The relatively low process temperatures ($\approx$470 °C) ensure that no chromium reduction occurs as a result of precipitation formation.[5,6] The hard layer produced during diffusion treatment exhibits an expanded fcc lattice supersaturated with carbon and/or nitrogen, which is also referred to as expanded austenite.[4,5,7]

Due to these layer properties, for example, watch cases made of superaustenitic stainless steels are treated with such a process as a very good scratch and corrosion resistance (body sweat) with an antiferromagnetism or paramagnetism is required. However, during a particular low-temperature carburization process, a clear magnetizability was detected as a case of damage in exactly such a watch case. Based on this unique detection, an extensive experimental investigation of these magnetic effects was subsequently initiated.

Ferromagnetic layer properties on expanded austenite produced by low-temperature nitriding were already described in 1986.[8] Furthermore, recent investigations show ferromagnetism on nitrided steels of the quality AISI 316 and AISI 316L.[9–11]

Ferromagnetism in carbon-expanded austenite, which is the subject of this work, has been studied only rarely and, therefore, defines a new field of research. The lower solubility of carbon in

austenite with the associated lower lattice expansion, which is assumed to be the cause of the occurring ferromagnetism, should be a reason against its occurrence. Nitrogen has generally a higher affinity to chromium than carbon, which can be considered as another reason for the lower carbon absorption.[12,13]

In the case of nitrogen-expanded austenite, a notable change in the lattice parameter was observed with a smaller change in the nitrogen content.[14] In this work, Brink et al. recognized a dependence between this lattice parameter variation and the transition of para- to ferromagnetism.[15] For the transition from para- to ferromagnetism, a certain interstitial nitrogen content is required, which triggers the ferromagnetism and an expansion excess/volume jump, similar to the anti-invar alloys.[9,15,16]

The current work is aimed at a fundamental investigation of ferromagnetic effects on carbon-expanded austenite. Nine different austenitic steels were investigated to be able to deduce any alloying influence. In the following, only three alloys are discussed here as examples and are representative for alloys that show no, medium, and strong magnetization after treatment.

2. Experimental Section

2.1. Alloy and Sample Preparation

The samples were provided as rolled plate samples in the solution-annealed condition. Prior to heat treatment, the specimens were wet-ground on both sides (grit P1200) and subsequently subjected to industrial low-temperature carburization (Kolsterizing). To reach massive carbon supersaturation of the austenitic fcc lattice, surface oxidation and carbide formation need to be suppressed. Therefore, the process is generally conducted at a rather low temperature (between 400 and 500 °C) using a process conditions that activate the surface; that is, the passivating chromium oxide layer is removed, e.g., by means of a standard double HCL process.[6,7] At the same time, a gaseous process provides the carbon and/or nitrogen for the diffusion process.[4,6,17]

The chemical compositions of the steels considered here are given in **Table 1** as the result of a spectral analysis.

The alloys presented here include one metastable (A) and two superaustenitic alloys (B and C). All samples of the individual alloys were treated multiple times (once and twice) with the Kolsterising heat treatment applied industrially by the company Bodycote GmbH, to achieve a higher carbon absorption with a longer diffusion time. In the sample identification number, the alloy letter is followed by a number that provides information on the number of treatments of the sample (once/1× or twice/2×); that is, the sample designation B2 indicates that it is alloy B (1.4539) which was treated twice.

2.2. Magnetization

Magnetizability was determined using a Feritsope (Fischer Dualscope FMP100) on 30 mm × 30 mm sheet samples after heat treatment. Prior to each measurement, the instrument was calibrated with calibration standards. The magnetizability determined in the measurement volume is given as equivalent ferrite content (**Table 2**).

2.3. Layer Characterization

The characterization of the layer in this work is based on light optical microscopy (LOM, Olympus BX51M) of metallographic cross-sections and microhardness testing (Leica VM HTMOT). The layer was made visible by immediate immersion of the metallographic cross-section after the final polishing step (0.25 μm diamond suspension) in V2A etchant (100 ml HCl (37 %) and H_2O, 10 ml HNO_3 (65 %), 0.3 ml Dr. Vogels Sparbeize; 60 °C@70 s); see **Figure 1**.

2.4. X-ray Diffraction (XRD) Analysis of the Expanded Austenite

The lattice expansion resulting from the interstitially dissolved carbon was determined by direct measurement of the lattice parameter using XRD, which was performed in collaboration with the Denmark Technical University (DTU). High compressive residual stresses were detected in the samples and a maximum information depth of 0.5 μm could be ensured.[5,14,18] Therefore, a very exact determination of the lattice planes as well as of the lattice parameter was possible.

2.5. C Profile Analysis by Glow Discharge Optical Emission Spectroscopy (GDOES)

The carbon absorption of the ferromagnetic samples was calculated based on the lattice parameters determined by XRD and can be interpreted as the maximum values of the outermost surface zone (max. 0.5 μm). To get a comparison with the actually dissolved carbon content, GDOES depth profile analyses were conducted. The measured carbon content was used to calculate the corresponding lattice parameter. The measurements were

Table 2. Equivalent ferrite content of the samples after Kolsterizing.

Sample/alloy	Untreated [Fe%]	Treated once [Fe%]	Treated twice [Fe%]
A/1.4404 1	0.0	0.0	0.0
B/1.4539	0.0	3.3 ± 0.03	9.0 ± 0.08
C/1925hMo	0.0	5.0 ± 0.04	13.8 ± 0.18

Table 1. Chemical compositions of the alloys.

Sample/alloy	C [wt%]	Cr [wt%]	Ni [wt%]	Mo [wt%]	Mn [wt%]	Si [wt%]	Cu [wt%]	Co [wt%]	Ti [wt%]	N [wt%]
A/1.4404	0.03	17.72	11.18	2.11	1.51	0.60	0.43	0.19	0.01	0.07
B/1.4539	0.02	20.75	24.26	4.72	1.62	0.22	1.31	0.13	0.01	0.05
C/1925hMo	0.02	20.41	24.34	6.14	0.84	0.32	0.83	0.17	0.02	0.10

**ADVANCED
SCIENCE NEWS**

www.advancedsciencenews.com

**steel
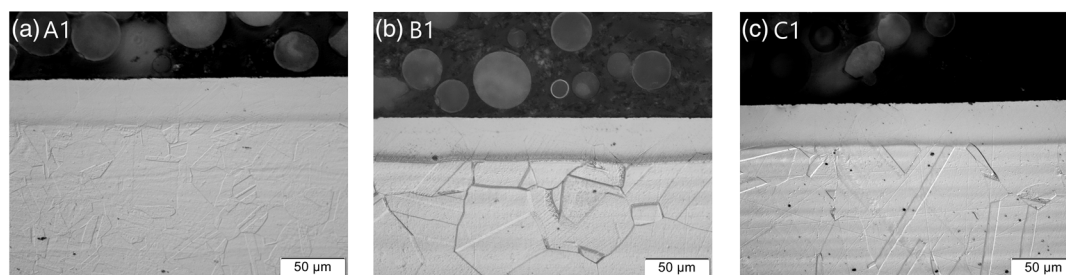research**
international

www.steel-research.de

Figure 1. Cross-sections with layer thickness after Kolsterizing once (etched state), a) alloy 1.4404, b) alloy 1.4539, and c) alloy 1925hMo.

conducted in close cooperation with the manufacturer of the GDOES equipment, Spectruma Analytik GmbH, up to a layer depth of 100 μm.

2.6. Grain Orientation Dependence of Magnetization

The ferromagnetic surface layer and the cross-sections of the magnetizable alloys B and C were examined using magnetic force microscopy (MFM) and a ferrofluid. Ferrofluid consists of fine magnetic particles that are dispersed in an oily carrier liquid and tend to enrich on top of ferromagnetic areas. This enables the ferromagnetic domains to be imaged with a conventional light microscope and in a similar way to the MFM measurements.

Different types of ferromagnetic regions in different grains were found, which change at grain boundaries. For the investigation of grain orientation dependencies, two different scanning electron microscopes (SEMs) in combination with electron backscatter diffraction (EBSD) were used. Primarily, grain regions with a pronounced magnetic domain structure, as previously confirmed by the ferrofluid or MFM, were examined with EBSD (Zeiss Sigma VP series SEM with EDAX EBSD TEAM Octane Plus-DigiView [Figure 6]; Zeiss GeminiSEM 300 with Oxford Symmetry EBSD-Camera [Figure 7 and 8]) were used. Using electron channeling contrast imaging (ECCI), the investigation of lattice defects was conducted using the same SEM and a four-quadrant backscatter electron detector (BSE), in which the detector fields were inverted as required for better imaging of these lattice defects. For the MFM investigations, a Bruker MultiMode atomic force microscope (AFM) equipped with a magnetic scanning tip from TEAM NANOTEC type HR-MFM 225C3.0-ML1-R was applied.

3. Results and Discussion

The three alloys discussed in this article represent the magnetizability correlations detected in the complete sample range. It should be mentioned in advance that alloy A shows no magnetizability at all, irrespective of the treatment condition, whereas alloys B and C show a clear magnetizability, which increases with each further treatment (see Table 2). The effect of an increasing magnetizability was also observed with more than two multiple treatments.

3.1. Magnetization and Layer Characterization

By means of the Feritscope measurements, the magnetizability was determined on the Kolsterized layer surface of the fully austenitic samples in terms of equivalent ferrite content. Table 2 shows the average values from ten individual measurements. The magnetizability determined in the measured volume is given as the equivalent ferrite content in percentage.

The measurement results in Table 2 show that there is an alloy influence on the formation of ferromagnetism. Alloy A shows no magnetizability at all regardless of multiple treatments, whereas it is clearly present in alloys B and C after only one treatment and increases further with the second treatment. A difference in magnetizability (equivalent ferrite content) between alloys B and C could also be detected after the individual treatments.

The layer thicknesses measured by an optical light microscope are shown for the example on of the simply treated samples in Figure 1. These results were very similar for the double-treated samples.

The determined layer thicknesses are shown in **Table 3**, which summarizes the results of this investigation. A layer thickness increase was detected by the twice-treated samples, whereby all three alloys tend to a similar layer-thickness formation.

The hardness profiles measured on the cross-sections are not explained in more detail here. It remains to be seen that multiple treatment has almost no influence on the maximum hardness (**Figure 2**). The higher alloyed steels B and C, which exhibit ferromagnetism after heat treatment, have a slightly higher maximum hardness ≥900 HV0.025 compared to steel A ≤ 800 HV0.025.

3.2. Lattice Expansion

In the this work, it was demonstrated that an expansion of the austenite lattice, caused by interstitial dissolved carbon in the lattice, can lead to ferromagnetism. On one hand, this was shown

Table 3. Result of the layer thickness determination using light optical microscopy.

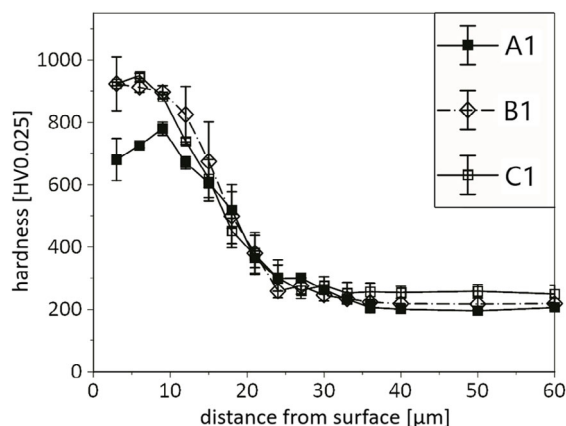| Sample/alloy	Treated once [μm]	Treated twice [μm]
A/1.4404	27 ± 0.6	40 ± 0.9
B/1.4539	30 ± 1.1	37 ± 2.2
C/1925hMo	28 ± 0.3	36 ± 0.7

Figure 2. Hardness profiles (HV0.025) of the samples A1 (1.4404), B1 (1.4539), and C1 (1925hMo) after Kolsterizing once.

Table 4. Lattice parameter determination from XRD measurements with conversion to other characteristics of carbon expanded austenite.

Sample/alloy	Characteristics	Untreated	Treated once	Treated twice
A/1.4404	Lattice parameter (a):	3.601 Å	3.690 Å	–
	Interstitial C content:	–	$\gamma_C = 0.15$	–
	Atomic percentage:	–	12.9 at%	–
	Lattice expansion:	–	2.47%	–
B/1.4539	Lattice parameter (a):	3.602 Å	3.739 Å	3.743 Å
	Interstitial C content:	–	$\gamma_C = 0.23$	$\gamma_C = 0.23$
	Atomic percentage:	–	18.5 at%	19.0 at%
	Lattice expansion:	–	3.80%	3.91%
C/1925hMo	Lattice parameter (a):	3.600 Å	3.738 Å	3.742 Å
	Interstitial C content:	–	$\gamma_C = 0.23$	$\gamma_C = 0.24$
	Atomic percent:	–	18.6 at%	19.1 at%
	Lattice expansion:	–	3.83%	3.94%

by the lattice parameters determined by XRD measurements, which reveal a clear lattice expansion after low-temperature carburizing—alloy A (1.4404): $a_0 = 3.601$ Å and $a_1 = 3.690$ Å; alloy B (1.4539): $a_0 = 3.602$ Å, $a_1 = 3.739$ Å, and $a_2 = 3.743$ Å; alloy C (1925hMo): $a_0 = 3.600$ Å, $a_1 = 3.738$ Å, and $a_2 = 3.742$ Å.

The determined lattice parameters represent the outermost surface layer (depth < 0.5 μm). Here, a pronounced lattice expansion (e.g., 3.602–3.743 Å) was measured for all alloys, but it is larger for the higher-alloyed austenitic alloys (B and C) than for alloy A.

The lattice expansion caused by the carbon uptake can be used to mathematically estimate the interstitially dissolved amount of carbon. In this regard, a linear relationship between the lattice parameter and the occupancy of the octahedral interstitial lattice sites was recognized in an earlier work on thin foils made of a stainless steel grade 1.4401/AISI 316.[12,14] Since then, some researchers have used the dimensionless parameter $\gamma_{N/C}$ as a measure of the dissolved content of nitrogen and/or carbon and referred to it as the "interstitial content," which corresponds to the number of carbon atoms to the number of metal atoms in an fcc lattice structure. To allow a direct comparison of the results from these works, the parameter $\gamma_{N/C}$ is also used here. The γ_C value can be calculated according to Equation (1) and has so far only been proven for a γ_C value of up to 0.16.[12]

$$a(C) = 3.5965\,[\text{Å}] + (0,6029 \pm 0,0189) \times \gamma_C \qquad (1)$$

In this work, Equation (1) was used with the initial lattice parameter. The reference value of $a_0 = 3.5965$ Å was replaced by the lattice parameters of the untreated samples determined by XRD measurements. According to the equation $X_C = \gamma_C/(1 + \gamma_C)$, the interstitially dissolved carbon content (γ_C) introduced during the process can also be converted into atomic percentage.[19] For alloy A without ferromagnetism, the interstitial carbon content in the once-treated state is $\gamma_{C\text{-}A1} = 0.148$, which corresponds to a lattice expansion of 2.5%. The two alloys with ferromagnetism (B and C) show significantly higher values here and are almost identical with respect to the percentage lattice expansion (**Table 4**).

The lattice parameters determined by XRD and the carbon absorption of the ferromagnetic samples are maximum values of the outermost edge zone (max. 0.5 μm). To obtain a comparison with the real carbon content, GDOES depth profile analyses were conducted, which allowed the corresponding lattice parameter to be calculated (**Figure 3**).

The lattice parameters of the GDOES analyses listed in **Table 5** are representative for a layer depth of 0.15–0.5 μm.

The lattice parameters determined from the GDOES analysis, which were calculated from the measured carbon content, correlate with the lattice parameters from the XRD measurements. This confirms the lattice expansion to be correlated directly with the interstitially dissolved carbon atoms.

From the investigations on the cross-sections by means of MFM and the ferrofluid, it is evident that not the entire layer of the expanded austenite exhibits ferromagnetic properties. Approximately 20–30 % of the outermost edge layer (see **Figure 4**) shows ferromagnetism. A similar characteristic has already been proven for ferromagnetism in nitrogen-expanded austenite.[9,20]

With increasing layer depth, a lower lattice parameter is present. The thickness of the ferromagnetic layer at the cross-sections is significantly smaller than the thickness of the hardened zone detected by light microscopy. This suggests that ferromagnetism can be expected when a lower lattice parameter ($a_{\text{ferro-min}}$) threshold is exceeded, compared to the values mentioned previously. Therefore, the ferromagnetic layer thickness was determined on the cross-sections using MFM and the ferrofluid. With these values, the carbon content at the corresponding layer depth was determined from the GDOES depth profile analyses and was finally used to calculate the lattice parameter ($a_{\text{ferro-min}}$). The lattice parameter curves calculated from the GDOES profiles and the determination of the minimum required lattice parameter $a_{\text{ferro-min}}$ are exemplary shown in Figure 4.

For alloy B (mean value for B1 and B2) and alloy C (mean value for C1 and C2), the $a_{\text{ferro-min}}$ values amount to
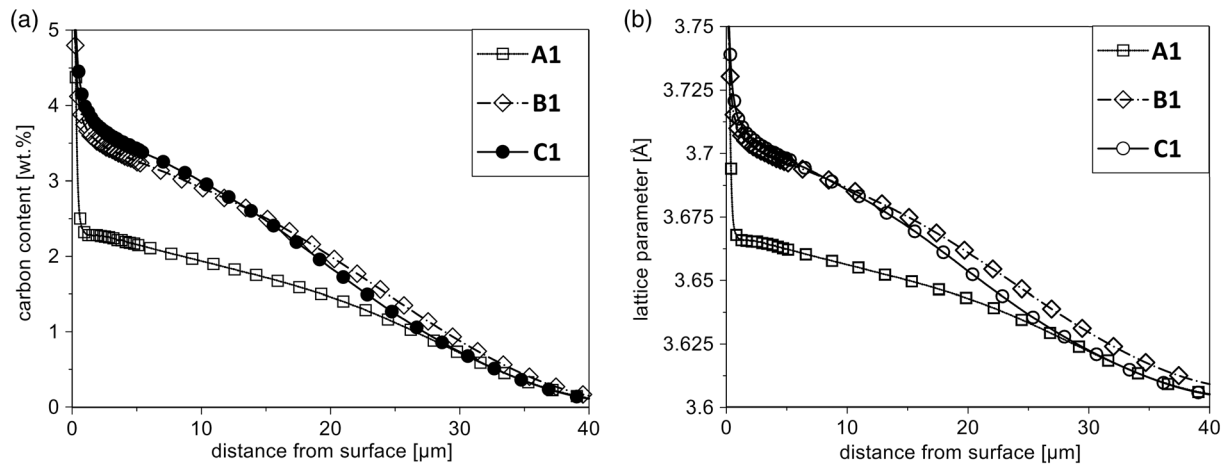
Figure 3. a) GDOES depth profile (carbon content) and b) calculated corresponding lattice parameter.

Table 5. Comparison of lattice parameters, calculated from GDOES depth profile analysis (mean value over a layer depth of 0.15–0.5 μm) with XRD lattice parameters.

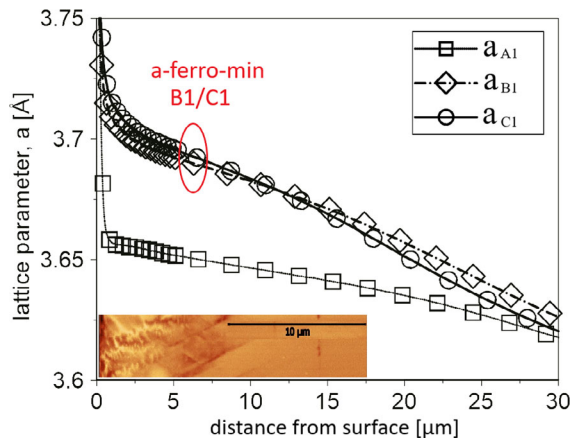| Sample/alloy	Treated once GDOES/XRD [Å]	Treated twice GDOES/XRD [Å]
A/1.4404	a: 3.704/3.690	a: 3.699/–
B/1.4539	a: 3.732/3.739	a: 3.733/3.743
C/1925hMo	a: 3.743/3.738	a: 3.749/3.742

Figure 4. Lattice parameter versus distance from surface with the ferromagnetic layer thickness shown schematically, including the minimum necessary lattice parameter ($a_{\text{ferro-min}}$). The lattice parameter profile was calculated based on the GDOES depth profile analysis.

$$a_{\text{ferro-min-B}} = 3.691\,\text{Å}$$
$$\left(\gamma_{\text{C,B-ferro-min}} = 0.149;\ 13.0\,\text{at.\%};\ \text{lattice expansion}: 2.5\%\right) \quad (2)$$

$$a_{\text{ferro-min-C}} = 3.695\,\text{Å}$$
$$\left(\gamma_{\text{C,C-ferro-min}} = 0.154;\ 13.4\,\text{at.\%};\ \text{lattice expansion}: 2.6\%\right) \quad (3)$$

The minimum necessary lattice parameters $a_{\text{ferro-min}}$ determined on the alloys with ferromagnetic layer properties

correspond to the lattice parameter, which was determined in similar dimensions in the outermost edge region of the alloys and which does not become ferromagnetic (compared to lattice parameter $a_1 = 3{,}690\,\text{Å}$). Therefore, an additional alloy influence on the formation of ferromagnetism can be assumed, which seems to depend fundamentally on the lattice expansion.

Thus, the extent of expanded austenite in these two alloys lies in a range, which has not yet been observed for interstitially dissolved carbon. The previously only theoretically assumed course for carbon-expanded austenite above the previously described limit value of $\gamma_C = 0.16$ (dashed line) could be reproduced precisely on the basis of the diagram by Brink et al. (**Figure 5**).[12,15]

Christiansen et al. describe a maximum interstitial content of $\gamma_C = 0.22$ for carbon-expanded austenite, which was obtained by a lattice expansion without referring to ferromagnetism.[19] In both publications, very fine powders or very thin foils (5 and 7.5 μm) were used. Based on the lattice parameters determined for the carbon-expanded austenite, the observed ferromagnetism can be justified, although the ferromagnetism here is
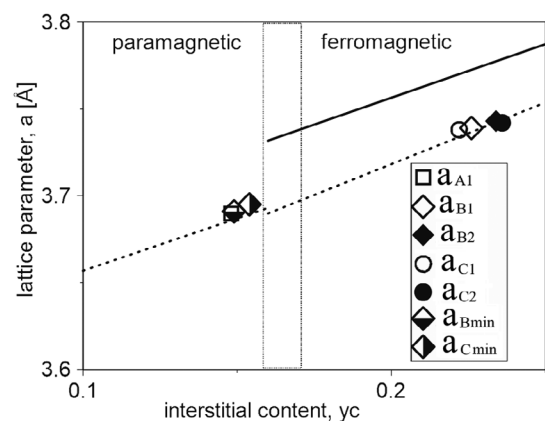

Figure 5. Lattice parameter versus interstitial carbon content (γ_C) and the transition region from para- to ferromagnetism according to Brink et al.[15] Solid lines γ_N, dashed lines γ_C. B_{min} and C_{min} correspond to the minimum necessary γ_C value determined for the occurrence of ferromagnetism in alloy B and C (see Figure 6).

**ADVANCED
SCIENCE NEWS**

www.advancedsciencenews.com

**steel
research**
international

www.steel-research.de

accompanied by a different form of lattice expansion as compared to the nitrogen-expanded austenite. The transition from para- to ferromagnetism is described accordingly by Brink et al. from an interstitial nitrogen content of $\gamma_{N/C} = 0.17$ (14.5 at%; lattice expansion: 4.2%). In addition, the lattice jump is caused by the occurring ferromagnetism.[15] The lattice jump was already recognized by different authors.[12,18] Basso et al. and Wu et al. state a content of ~14 at% ($\gamma_N = 0.16$) of nitrogen for the occurring ferromagnetism.[9,11] The minimum required nitrogen content corresponds to the minimum required carbon content, without the onset of the lattice jump as in the case of nitrogen. It is possible that in the present specimen shape, the volume expansion of the layer is strongly inhibited by the constraint of the base material, whereby the resulting high residual compressive stresses are relieved by plastic deformation.[14,21] Corresponding values have not yet been detected for interstitially dissolved carbon with developed ferromagnetism. The lack of detection is justified by the low solubility of carbon compared to nitrogen and also the lower affinity of carbon to chromium.[12,22]

3.3. Grain Orientation Dependence

The ferromagnetic layer formed on the cross-sections of magnetizable alloys B and C was examined by MFM. Different characteristics of the ferromagnetic regions were found, which can be differentiated by the grain orientation.

Volume-defined areas with fine ferromagnetic domains can be observed, which partly show a labyrinthine structure (**Figure 6** and **7**). Furthermore, line structures were detected, presumably deformation twins with spatially narrow limited magnetizability. Such patterns can be mainly found in alloy B but can also be seen in alloy C (see Figure 6b,c). For sample B2, a very fine labyrinthine domain structure was discovered superimposed in the near-surface region. But nevertheless, this domain was much less pronounced compared to sample C2 (Figure 6d). In sample C2 (Figure 6d), the labyrinthine domain structure is dominating a larger area and shows no disturbance by line structures. Furthermore, the domain structure seems to change at the grain boundaries, supporting a grain-orientation-dependent ferromagnetic domain structure formation.

For further visualization of the magnetic structure, the Kolsterized surfaces were treated with a ferrofluid. The magnetizable areas could then be detected with a conventional light microscope. The magnetizable areas identified by this technique were then examined in more detail using MFM, and the respective grain orientation was determined with a subsequent EBSD measurement. The results of the samples C1 (Figure 7) and C2 (**Figure 8**) are presented exemplarily.

In the area of the <001> orientation, larger-volume grain areas (massive domain areas) with a labyrinthine ferromagnetic domain structure were detected, which is consistent with ferromagnetism in all investigated sample surfaces of the alloys. This "massive-domain structure" was also detected on the cross-sections solely in grain regions, which were not disturbed
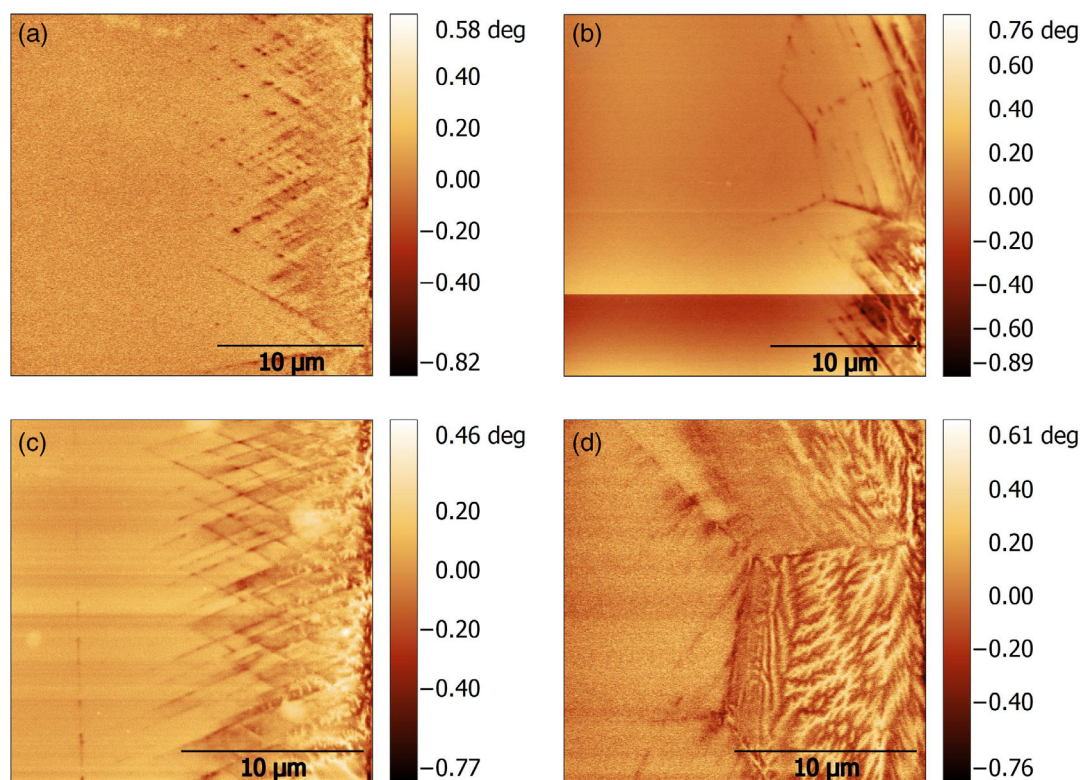

Figure 6. MFM investigations to visualize the magnetic domain structure on cross-sections of the samples, a) B1: 1.4539 treated once, b) C1: 1925hMo treated once, c) B2: 1.4539 treated twice, and d) C2:1925hMo treated twice.
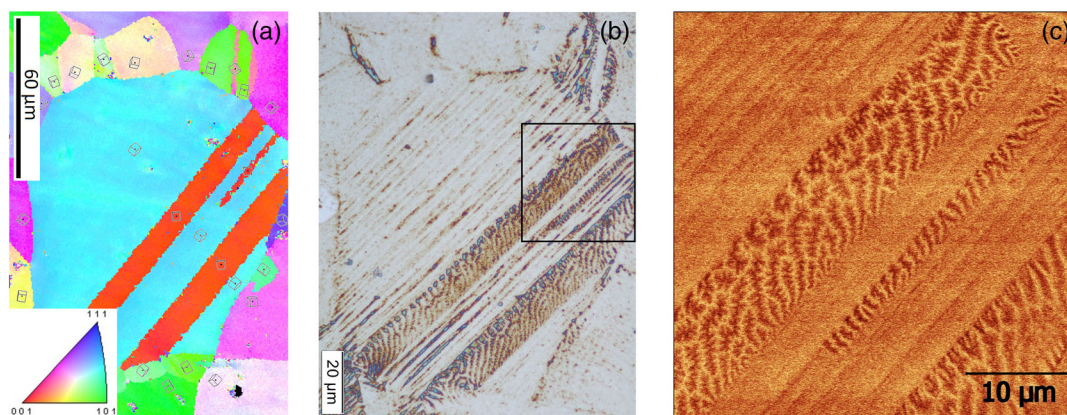
**ADVANCED
SCIENCE NEWS**

www.advancedsciencenews.com

**steel
research**
international

www.steel-research.de

Figure 7. Grain-orientation-dependent magnetic domain formation on the carburized surface of sample C1, a) EBSD orientation mapping (IPF coloring), b) ferrofluid examination on optical light microscope with marked detail area for MFM examination, and c) MFM examination of detail area in (b).
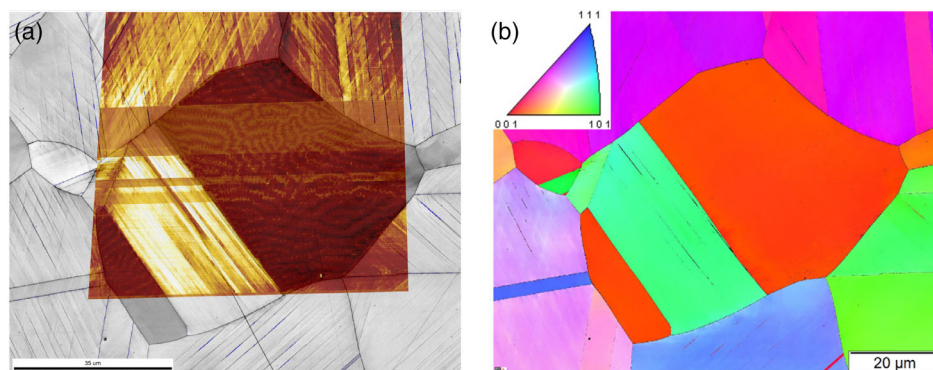

Figure 8. Sample C2, a) EBSD (band contrast) with superimposed MFM measurement; b) EBSD orientation mapping (IPF coloring).

by linear lattice defects (microtwins or slip traces). At the interfaces and intersections of the linear lattice disorder, ferromagnetism was also detected. In the samples C1 and C2, increasing linear defects were found in the grain orientations that deviate significantly from the <001> orientation.

On the basis of the EBSD and ECCI examinations, the linear defects in sample C2 (**Figure 9**a,b) were assigned mainly to microtwins in the grain regions without pronounced magnetic domain structure. In the <001> orientation, almost no plastic

deformations were detected, in contrast to other deviating orientations.

The detected twins were found to be ferromagnetic at the interfaces and intersections. It was proven that the reason for the ferromagnetism is the interstitially dissolved carbon in combination with the lattice expansion in the austenite only. As no stress-induced martensite or precipitations were detected by any examination method, such effects were excluded as a potential reason for the observed magnetizability. A distinction was made
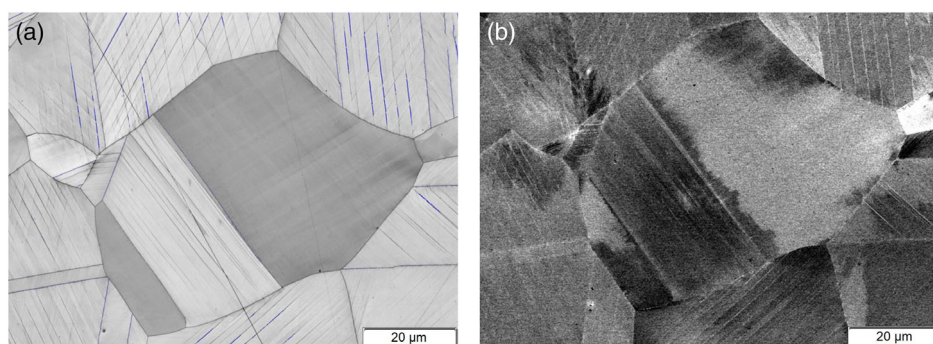

Figure 9. Sample C2, a) EBSD (band contrast) and b) ECCI.

2100272 (7 of 9)

in the appearance of the magnetic domains. Only in the <001>-oriented grains, the labyrinthine domain structure was found during the surface layer examinations. In the case of deviating orientations, there were other lattice disturbances, presumably deformation twins or slip traces with no or less labyrinthine domain structure.

The expansion of the austenite lattice due to the massive carbon intercalation and the suppressed volume expansion through the base material leads to high compressive residual stresses in the layer.[18] This results in plastic deformations, especially lattice defects, such as twins and plastic glide on crystalline slip planes, which was detected in large numbers outside the <001> orientation. As no lattice defects and the distinct magnetic domains were detected in the <100> orientation, it is suspected that greater lattice expansion is achieved in this superficial grain orientation due to the lack of plastification. A previously observed elastic and plastic anisotropy has already been described by means of nitrogen-expanded austenite.[23–25] The correlations identified in these works, for example, with regard to plastic deformations, cannot be applied to the specimens investigated herein. The grain-orientation-dependent formation of lattice defects in correlation with the local lattice parameters are currently subject of further high-resolution TEM measurements.

From the investigated alloy dependence, a further approach can be suggested, which reveals the stacking fault energy (SFE) of the base material and the associated plastic deformation behavior as an influencing variable. The SFE according to Pickering (Equation (4)) was used for evaluation as it takes into account the main alloying elements and the alloys with high manganese and nitrogen content.[26]

$$
\begin{aligned}
\text{SFE}\left(\frac{mJ}{m^2}\right) = {}& 25.7 + 2 \times (\%\text{Ni}) + 410 \times (\%\text{C}) - 0.9 \times (\%\text{Cr}) \\
& - 77 \times (\%\text{N}) - 13 \times (\%\text{Si}) - 1.2 \times (\%\text{Mn})
\end{aligned}
$$

(4)

Thus, all the alloys used can be evaluated identically, even though the formula was not developed on the basis of the alloying elements used. This possible influence and the related plastic deformation behavior in the layer will not be discussed further here and will form the basis for a further project.

Similar to classical heat treatment, a distinction can be made here between a dimensional change caused by irritated atoms which is definitely hindered in a multicrystal, and a change in the shape of the crystal caused by microdeformation. This is a possible explanation for the observed influence of the alloy on the layer magnetization behavior of the carburized surface. Especially the superaustenitic stainless steel alloys show a significant magnetizability after heat treatment.

4. Conclusion

Ferromagnetism was detected in carbon-expanded austenite, depending on the alloy composition, where the interstitially dissolved carbon content was determined to be 13–19 at% ($\gamma_C = 0.15$–0.24). Furthermore, it was found that only 20–30% of the total layer thickness was relevant for ferromagnetism.

The ferromagnetic areas manifest themselves by the appearance of domain structures that were visualized on metallographic cross-sections of the Kolsterized-expanded austenite layer. By using a ferrofluid and MFM, different forms of magnetic domains were detected, which depend on the local crystallographic orientation. Especially the surface layer investigations have proven that <001>-oriented grains can almost exclusively be assigned a massively occurring labyrinthine domain structure. A locally reduced formation of ferromagnetism was correlated with the appearance of twin and slip lines in grains of an orientation deviating from the <001> orientation. This was supported by the EBSD and ECCI measurements and supports the hypothesis that local plasticity limits locally high compressive stress and ferromagnetism accordingly. The ferromagnetism occurs due to the interstitially dissolved carbon and the resulting lattice expansion in a similar way as it was found in nitrogen-expanded austenite in earlier work. As large-scale plastic deformation seems to have a strong effect on the occurrence of ferromagnetism in austenitic steel, the SFE was taken into account to understand the effect of the alloy chemical composition. The SFE is a measure of the nature of plastic deformation, that is, transformation induced plasticity (TRIP), twinning induced plasticity (TWIP), or dislocation gliding, being responsible for stress relief. Accordingly, only a few specifically oriented grains achieve the necessary lattice size for the formation of significant ferromagnetic domains, whereas the grains with a different orientation show little or no domain structure.

Conflict of Interests

The authors declare no conflict of interest.

Data Availability Statement

Research data are not shared.

**ADVANCED
SCIENCE NEWS**

www.advancedsciencenews.com

**steel
research**
international

www.steel-research.de

[1] W. Weißbach, *Werkstoffkunde. Strukturen, Eigenschaften, Prüfung*, Friedr. Vieweg & Sohn Verlag GWV Fachverlage GmbH, Wiesbaden **2007**.

[2] P. Gümpel, *Rostfreie Stähle. Grundwissen, Konstruktions- und Verarbeitungshinweise*, Vol. 7, Expert-Verlag, Renningen **2008**, pp. 693–716.

[3] B. H. Kolster, in *VDI-Berichte 506*, Conference paper, VDI-Verlag, Duesseldorf **1983**, pp. 107–113.

[4] E. J. Mittemeijer, M. A. J. Somers, (Hrsg.), *Thermochemical Surface Engineering of Steels: Improving Materials Performance*, Woodhead Publishing, Cambridge, MA **2015**.

[5] M. A. J. Somers, Ö. C. Kücükyildiz, C. A. Ormstrup, H. Alimadadi, J. H. Hattel, T. L. Christiansen, G. Winther, *Mater. Perform. Charact.* **2018**, *7*, 20170145.

[6] F. Ernst, A. Avishai, H. Kahn, X. Gu, G. M. Michal, A. H. Heuer, *Metall. Mater. Trans. A* **2009**, *40*, 1768.

[7] F. Ernst, Y. Cao, G. M. Michal, *Acta Mater.* **2003**, *51*, 4171.

[8] K. Ichii, K. Fujimura, T. Takase, in *Structure of the Ion-Nitrided Layer of 18-8 Stainless steel*, Vol. 27, Technology Reports of Kansai University, **1986**, pp. 135–145.

[9] R. L. O. Basso, V. L. Pimentel, S. Weber, G. Marcos, T. Czerwiec, I. J. R. Baumvol, C. A. Figueroa, *J. Appl. Phys.* **2009**, *105*, 124914.

[10] M. Olzon-Dionysio, D. Olzon-Dionysio, M. Campos, W. Takemitsu Shigeyosi, S. Dionysio de Souza, S. de Souza, *Hyperfine Interact.* **2019**, *240*, 26.

[11] D. Wu, H. Kahn, G. M. Michal, F. Ernst, A. H. Heuer, *Scr. Mater.* **2011**, *65*, 1089.

[12] T. S. Hummelshøj, T. L. Christiansen, M. A. J. Somers, *Scr. Mater.* **2010**, *63*, 761.

[13] Ö. C. Kücükyildiz, F. B. Grumsen, T. L. Christiansen, G. Winther, *Acta Mater.* **2020**, *194*, 168.

[14] T. L. Christiansen, M. A. J. Somers, *Metall. Mater. Trans. A* **2006**, *37*, 675.

[15] B. K. Brink, K. Ståhl, T. L. Christiansen, C. Frandsen, M. F. Hansen, M. A. J. Somers, *Acta Mater.* **2016**, *106*, 32.

[16] W. Pepperhoff, M. Acet, *Konstitution und Magnetismus des Eisens und seiner Legierungen*, Springer Verlag, Berlin, Heidelberg **2000**.

[17] M. A. J. Somers, T. L. Christiansen, PCT patent application WO2006136166, **2005**.

[18] K. V. Werner, Master Thesis, DTU, **2019**.

[19] T. L. Christiansen, K. Ståhl, B. K. Brink, M. A. J. Somers, *Steel Res. Int.* **2016**, *87*, 1395.

[20] D. Wu, PhD Thesis, Case Western University, **2013**.

[21] Y. Peng, Z. Liu, Y. Jiang, B. Wang, J. Gong, M. A. J. Somers, *Scr. Mater.* **2018**, *157*, 106.

[22] T. L. Christiansen, M. A. J. Somers, *Int. J. Materi. Res.* **2009**, *100*, 1361.

[23] J. C. Stinville, P. Villechaise, C. Templier, J. P. Riviere, M. Drouet, *Surf. Coat. Technol.*, **2010**, *204*, 1947.

[24] F. Borgioli, *Metals* **2020**, *10*, 187.

[25] C. Tromas, J. C. Stinville, C. Templier, P. Villechaise, *Acta Mater.* **2012**, *60*, 1965.

[26] F. B. Pickering, in *Proc. of the Conf. Sponsored and Organised Jointly by Chalmers University of Technology and Jernkontoret (Sweden) with the Metals Society (UK)*, Chalmers University of Technology, Göteborg **1984**.